Formation of Defect-Free Polyetherimide/PIM-1 Hollow Fiber Membranes for Gas Separation

Lin Hao
Dept. of Chemical & Biomolecular Engineering, National University of Singapore, 4 Engineering Drive 4, Singapore 117585

NUS Graduate School for Integrative Sciences and Engineering, National University of Singapore, 28 Medical Drive, Singapore 117456

Jian Zuo and Tai-Shung Chung
Dept. of Chemical & Biomolecular Engineering, National University of Singapore, 4 Engineering Drive 4, Singapore 117585

DOI 10.1002/aic.14565
Published online July 28, 2014 in Wiley Online Library (wileyonlinelibrary.com)

Dual-layer hollow fiber membranes were produced from blends of Ultem and polymer of intrinsic microporosity (PIM-1) with enhanced gas permeance. The effects of spinning parameters (take-up speed and air gap distance) on gas separation performance were investigated based on the pristine Ultem. Selected spinning conditions were further adopted for the blend system, achieving defect-free and almost defect-free hollow fibers. Adding PIM results in a higher fractional free volume, 50% increments in gas permeance were observed for Ultem/PIM-1 (95/5) and more than 100% increments for Ultem/PIM-1 (85/15). Both O_2/N_2 and CO_2/CH_4 selectivities remained the same for Ultem/PIM-1 (95/5) and above 80% of their respective intrinsic values for Ultem/PIM-1 (85/15). The selective layer thickness ranges from 70 to 120 nm, indicating the successful formation of ultrathin dense layers. Moreover, minimum amounts of the expensive material were consumed, that is, 0.88, 1.7, and 2.3 wt % PIM-1 for Ultem/PIM-1 (95/5), (90/10), and (85/15), respectively. © 2014 American Institute of Chemical Engineers *AIChE J*, 60: 3848–3858, 2014
Keywords: membrane separations, hollow fibers, Ultem/PIM-1 blends, dual-layer, defect free

Introduction

Hollow fiber membrane is a proven technology for air separation, CO_2 capture as well as other gas separation.[1–4] To enhance gas transport, the active membrane layer should be uniform and thin, while the supporting layer must be mechanically strong to withstand high operation pressures but with minimal transport resistance.[4–8] To achieve this morphology and separation performance, the membrane can be designed by spinning asymmetric hollow fibers with an ultrathin selective skin and a porous support. Nevertheless, the formation of hollow fibers with a defect-free selective layer is always a challenge. Kesting et al. introduced the Lewis acid: base complex system in spinning dopes to form high performance polysulfone hollow fibers.[9] Chung et al. used a simplified method by forming Lewis acid: base complex dopes concurrently with polymerization (imidization) on their 6FDA-durene hollow fibers.[10] Koros and his coworkers developed the "dry/wet phase inversion" technology to produce defect-free hollow fibers without post-treatments.[5,11] All these studies reveal seven important consecutive steps in forming hollow fiber membranes; namely, dope preparation, degassing, metering, spinning, evaporation in the air gap region, coagulation in the wet phase inversion, and finally the solvent exchange.[12] Among them, the dope formulation, spinning conditions, and solvent exchange have dominant influence on the final morphology and gas transport properties of the fibers.

Besides the spinning process, treatments such as heat treatment or silicone rubber coating are often necessary to seal the defects and recover the gas-pair selectivity. Peng et al. spun Extem® under various spinning conditions and found this material could not form defect-free single-layer fibers without post-treatments.[13] However, additional post-treatments were undesirable as they would incur extra costs to membrane fabrication. Another technique of producing an ultrathin dense-selective layer is via dual-layer hollow fiber spinning, which had been successfully used for Extem® hollow fibers in the same study.[13] The dual-layer spinning technology was first invented by Yanagimoto for ultrafiltration[14] and was further developed by Ekiner et al. for gas separation.[15] Dual-layer asymmetric hollow fiber membranes are formed by coextrusion of two polymer dopes and one bore fluid through a triple-orifice spinneret.[4,6] Traditionally, low-cost polymers with high mechanical and thermal properties are chosen as the support layer while high performance materials are used as the outer selective layer.[16] Compared to single-layer hollow fibers, the production of dual-layer

Correspondence concerning this article should be addressed to T.-S. Chung at chencts@nus.edu.sg.

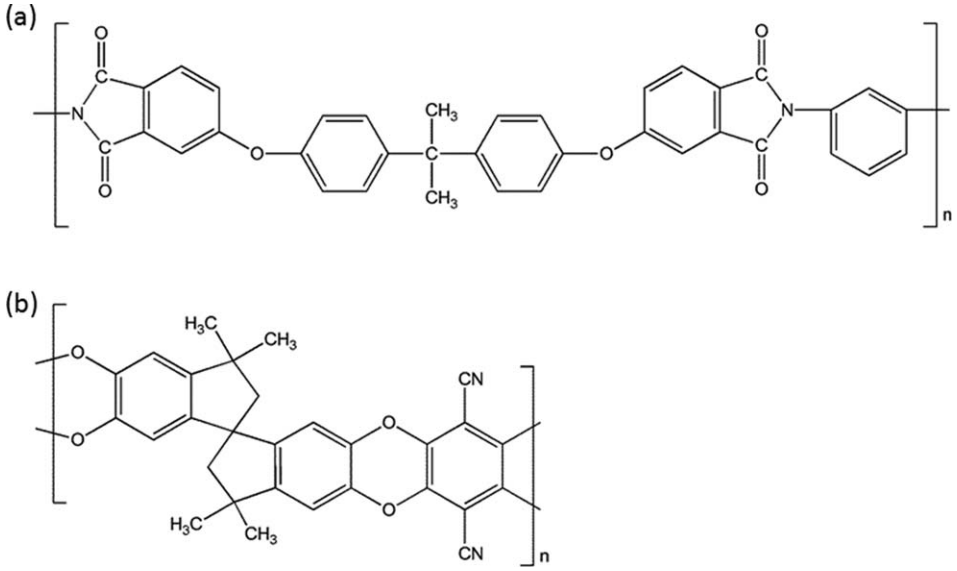

Figure 1. The chemical structures of (a) Ultem and (b) PIM-1.

hollow fiber membranes may eliminate the tedious post-treatment steps to form an active skin. In addition, the dual-layer configuration also significantly saves the material cost for the expensive outer selective layer.[12]

In this study, dual-layer hollow fiber membranes are fabricated with polymer blends of Ultem® 1010 (denoted as Ultem thereafter) and polymer of intrinsic microporosity (PIM-1) as the selective layer. Ultem is attractive for gas separation because of its good gas-pair selectivity[17,18] and chemical resistance.[19] In addition, it has higher plasticization pressure and is less costly compared to Matrimid.[20–23] Nevertheless, the low permeability has limited its applications as hollow fibers for gas separation. To enhance its gas separation performance, two approaches have been explored and both were based on the mixed-matrix membranes (MMMs) concept.[17,24,25] Husain et al. incorporated HSSZ-13 zeolite into the spinning dope and fabricated Ultem/zeolite mixed-matrix hollow fibers to enhance the membrane performance. However, the HSSZ-13 nanoparticles required special surface modifications which complicated the fabrication processes.[17,24] Dai et al. developed Ultem/ZIF-8 hollow fibers for CO_2/N_2 separation by embedding 13 wt % commercially available ZIF-8 particles in the outer-layer dope. After thermally treated at 75°C for 2 h, the resultant mixed-matrix hollow fiber has an 85% higher permeance and a 20% higher selectivity than the Ultem hollow fiber membrane.[25]

Different from their approaches, this study aims to develop a new type of high performance Ultem hollow fiber membranes based on the incorporation of PIM-1. This is due to the fact that our previous study showed that PIM-1 and Ultem easily formed partially miscible blends.[26] The Ultem/PIM-1 dense films display significantly improved gas transport performance compared to the pure Ultem films. Therefore, selected partially miscible blends are chosen in this study because we target to excel their permeance without compromising gas-pair selectivity for industrial interests and exploration. Compared to Matrimid/PIM-1 hollow fibers,[22] the Ultem/PIM-1 hollow fibers may be more applicable for precombustion and post-combustion CO_2 capture because the former has a less plasticization pressure and is more costly than the latter.

To minimize the usage of the expensive material (i.e., PIM-1) as well as to eliminate possible post-treatment steps, this work also aims to fabricate defect-free fibers directly from one-step dual-layer spinning. To overcome the delamination between the two layers and exploit Ultem's superior characteristics of chemical resistance and plasticization resistance, Ultem is chosen as the inner support layer to enhance interfacial adhesion with the outer Ultem/PIM-1 selective layer. A dry-jet wet spinning process is used to increase productivity and control fiber morphology. The effects of spinning conditions such as take-up speed and air gap distance on gas separation performance are investigated. This study may open up new applications and widen the potential for Ultem, PIM-1 as well as their blend hollow fibers.

Experimental

Materials

Ultem was ordered from the former GE Plastics. Figure 1a illustrates its structure. The PIM-1 monomers 5, 5′, 6, 6′-tetrahydroxy-3, 3, 3′, 3′-tetramethyl-1, 1′-spirobisinadane (TTSBI, 97%), and 2, 3, 5, 6-tetrafluoroterephthalonitrile (TFTPN, 99%) were obtained from Alfa Aesar and Matrix Scientific, respectively. Both anhydrous potassium carbonate (K_2CO_3, >99.5%) and lithium nitrate ($LiNO_3$, ReagentPlus®) were bought from Sigma-Aldrich and used without further purification. *N*-methyl-2-pyrrolidone (NMP, >99.5%), and methanol (MeOH, >99.9%) were acquired from Merck. Chloroform (99.98%), tetrahydrofuran (THF, 99.99%), and hexane (99.9%) were purchased from Fisher Scientific.

Synthesis of PIM-1 and preparation of Ultem/PIM-1 flat sheet membranes

PIM-1 was synthesized through polycondensation with stoichiometric TFTPN and TTSBI in anhydrous NMP.[27,28] This reaction was catalyzed by K_2CO_3 at 60°C under N_2 atmosphere for 18 h. The product was then precipitated,

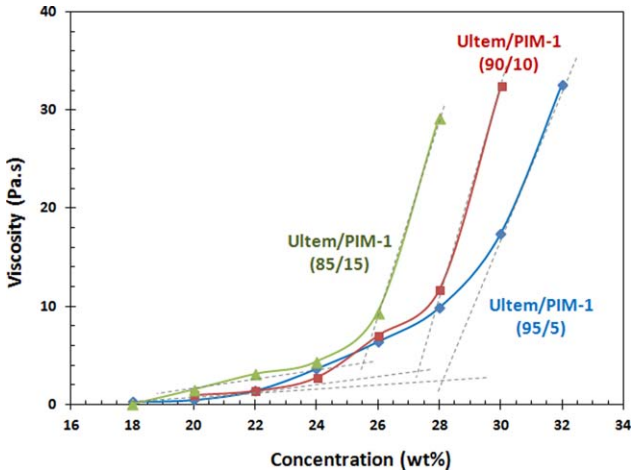

Figure 2. The critical concentrations of dopes with different component ratios.

[Color figure can be viewed in the online issue, which is available at wileyonlinelibrary.com.]

washed, and dried under vacuum with a yield of about 90%. The structure of PIM-1 is illustrated in Figure 1b.

Flat sheet Ultem/PIM-1 membranes with 5, 10, and 15 wt % PIM-1 loadings were prepared by a ring casting method using chloroform as the solvent.[26] The resultant membranes were dried at 120°C in a vacuum oven for future studies.

Spinning dope formation

In formulating spinning dopes, the concentrations of different polymer blends were first determined. For the porous inner support layer, an Ultem concentration of 23 wt % was chosen to provide both mechanical support as well as porous structure.[29]

For the outer selective layer, a 50/50 wt/wt NMP/THF mixture was used as the solvent to fully dissolve both components as well as to assist faster solvent evaporation in the air gap region during spinning. NMP is a strong solvent to Ultem and has a high boiling point. THF was chosen because it is a volatile solvent and has a high PIM-1 solubility while it is a nonsolvent to Ultem.[11] As a result, the rapid evaporation of THF would facilitate the formation of the ultrathin dense-selective layer.

Sufficient chain entanglement is one of the key factors in producing defect-free hollow fibers.[30] To form the ideal outer layer, the polymer dope has to reach certain viscosity. A lower concentration tends to reduce skin thickness and results in surface defects and a lower selectivity. As an empirical guide, the optimal polymer concentration is at or above its critical concentration.[31,32] Figure 2 shows the viscosity curves of polymer blends with PIM-1 loadings at 5, 10, and 15 wt %. The slopes of the curves become sharper beyond certain concentration ranges. The concentration at the crossed point of two extrapolation lines of their linear parts is identified as the critical concentration of this polymer solution.[12,13] For the pristine Ultem hollow fiber, the outer layer dope concentration was chosen to be above its critical concentration.[24,25]

Hollow fiber spinning

The well-dissolved dopes were allowed to degas for one day before being poured into the ISCO syringe pumps. Nascent hollow fibers were produced through a triple-orifice spinneret consisting of three channels.[6,33] The spinning process and spinneret design are illustrated in Figures 3a, b.

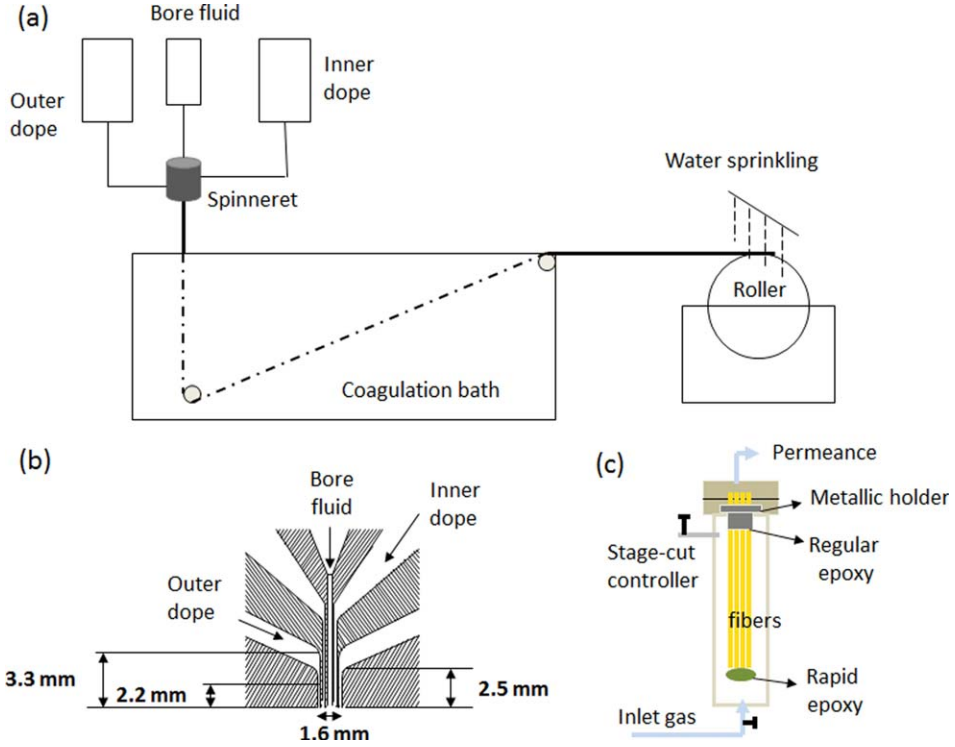

Figure 3. (a) Schematic diagram of the hollow fiber spinning line, (b) side view of the spinneret design, and (c) design of the testing chamber for hollow fiber modules.

[Color figure can be viewed in the online issue, which is available at wileyonlinelibrary.com.]

Table 1. The Spinning Conditions for Pristine Ultem Dual-Layer Hollow Fibers

Hollow Fiber ID	UA1	UA2	UB1	UB2	UC1	UC2	UD
Outer dope composition (wt %)	Ultem/NMP/THF/LiNO3 (30/34.5/34.5/1)						
Inner dope composition (wt %)	Ultem/NMP (23/77)						
Bore fluid composition (wt %)	NMP/water (95/5)						
External coagulant	Tap water						
Spinneret dimension (mm)	Dual-layer 1.6 no indent						
Spinning temperature (°C)	25 ± 2						
Outer dope flow rate (mL/min)	0.6	0.6	0.6	0.6	0.6	0.6	0.4
Inner dope flow rate (mL/min)	3.5	3.5	3.5	3.5	3.5	3.5	3.5
Bore flow rate (mL/min)	1.5	1.5	1.5	1.5	3	3	1.5
Air gap (cm)	7	7	10	10	4	4	10
Take-up speed (m/min)	16.2	21.8	21.8	27.3	21.8	27.3	21.8

The bottom side of the spinneret, where the dopes extrude, comprises three concentric circles: (1) the innermost channel is for the bore fluid containing various NMP/water mixtures, (2) the middle channel is for the inner dope consisting of Ultem, and (3) the outermost circle is for the outer dope comprising Ultem/PIM-1 blends. After being extruded from the spinneret, the nascent fiber was exposed to an air-gap region followed by a coagulation bath filled with tap water. The as-spun fibers were collected by a take-up roller and immersed in tap water for three days. Solvent exchange was performed three times in methanol for 1 h/time and another three times in *n*-hexane for 1 h/time to remove any residual NMP in the fibers. This solvent exchange process ensured the formation of an ultrathin selective layer.[11,34] The fibers were finally dried in air and vacuum for future investigation.

Table 1 lists the spinning conditions for the pristine Ultem. The bore fluid was chosen to be NMP/water (95/5) as high solvent content slows down the demixing as well as the precipitation of the inner surface. As observed by Yong et al. for Matrimid/PIM-1 single-layer hollow fiber membranes,[22] the fibers spun from a bore fluid concentration of 95 wt % NMP exhibited the most porous support structure and minimum gas transport resistance compared to those spun from bore fluids consisting of 80 or 50 wt % NMP. As literatures on Ultem fibers are limited, several parameters (i.e., outer-layer dope flow rate, take-up speed and air gap) were investigated first to obtain defect-free Ultem fibers. Their O_2/N_2 selectivity was examined to narrow down the workable conditions suitable for spinning Ultem/PIM-1 blending dopes. More details and rationales will be disclosed in later sections.

Characterizations

An Olympus BX50 polarized light microscope (PLM) was applied to analyze the homogeneity of flat sheet membranes and the images were further analyzed with Image Pro Plus 3.0 software. The cross-sectional images of hollow fibers were obtained via a field emission scanning electron microscope (FESEM), JSM-6700F. The hollow fibers were immersed and fractured in liquid nitrogen to prepare the SEM samples.

The glass transition temperatures (T_g) of different polymer blends were obtained using flat sheet blend membranes by a differential scanning calorimetry (DSC; Mettler Toledo DSC 822e, Columbus, OH). An X-ray diffractor (Bruker, D8 series, General Area Detector Diffraction System with a Cu Kα X-ray source (wavelength: 1.54 Å) was used to characterize the surface of Ultem hollow fibers and Ultem/PIM-1 (85/15) hollow fibers.

The structural changes, mainly the porosity change in the dense skin layer, were characterized by positron annihilation spectra (PAS).[22,33] In this process, a slow positron beam was accelerated by a mono-energy ranging from 0 to 27 keV. One of the Doppler broadening energy spectra parameter, *S*-parameter, was used to analyze the structural changes.[35]

Module preparation and permeance measurements

Eight to ten fibers with an average length of 16 cm were potted into one flat metallic hollow holder and glued by a regular epoxy resin with their ends open. The other end of the fibers was sealed by a using quick curing epoxy as shown in Figure 3c.[13,16] The pressure-normalized fluxes of the modules were tested in the order of N_2, O_2, CH_4, and CO_2 at ambient temperature with a transmembrane pressure of 300 kPa (3 bar). The module design for testing is illustrated in Figure 3c. The permeance, P/L, was calculated based on Eq. 1 below

$$\frac{P}{L}=\frac{273.15\times10^6}{T}\times\frac{Q}{n\pi Dl\Delta p} \tag{1}$$

where P/L is the permeance in GPU (P is the permeability, L refers to the dense-selective layer, 1 GPU = 1 × 10^{-6} cm^3 (STP)/cm^2 s cmHg), T is the testing temperature (K), Q refers to the gas flux (cm^3/s), n is the number of fibers in one module, D presents the outer diameter (cm), l is the effective length of the module (cm), and Δp refers to the pressure difference across the fiber (cmHg, 1 cmHg = 1.33 kPa). Three to four modules were prepared for each spinning condition and their averaged results were reported here. Mixed gas tests were conducted on Ultem/PIM-1 fibers comprising 10 and 15 wt % PIM-1 using a mixed gas of CO_2/CH_4 (50/50 mol %) with a CO_2 partial pressure of 300 kPa (3 bar). Sweep gas with a stage-cut of about 50 was applied to minimize the effects of concentration polarization.

The idea selectivity of the membranes, $\alpha_{A/B}$, was calculated as the ratio of the normalized fluxes shown in Eq. 2

$$\alpha_{A/B}=\frac{(P/L)_A}{(P/L)_B} \tag{2}$$

As it is difficult to measure the exact thickness of the dense-selective layer in hollow fibers, the thickness of the active layer is estimated according to Eq. 3 based on the permeance and permeability of O_2

$$L=\frac{P_{CO_2}(\text{dense film})\times10^7}{(P/L)_{CO_2}(\text{hollow fiber})} \tag{3}$$

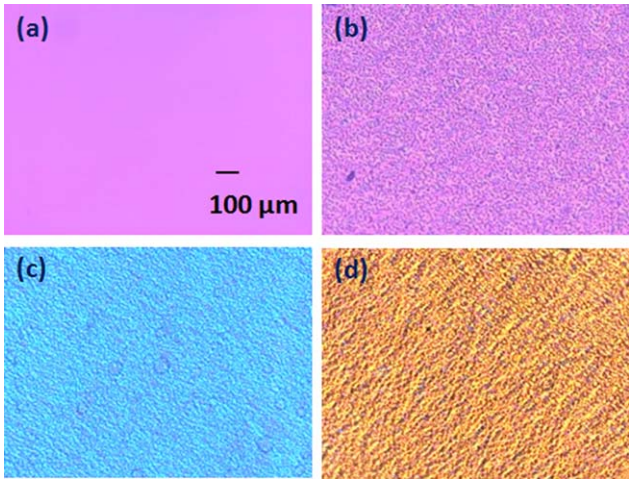

Figure 4. PLM images of flat sheet membranes with different component ratios with (a) Pristine Ultem, (b) Ultem/PIM-1 (95/5), (c) Ultem/PIM-1 (90/10), and (d) Ultem/PIM-1 (85/15).

[Color figure can be viewed in the online issue, which is available at wileyonlinelibrary.com.]

where L denotes the apparent selective layer (nm), P stands for the permeability in the flat sheet membrane in Barrer ($1\text{Barrer} = 3.348 \times 10^{-19}\text{kmol m/m}^2\text{s Pa}$).

Results and Discussion

Miscibility

PLM images of four flat sheet membranes with different PIM-1 loadings are presented in Figure 4. The images display homogeneous distribution of PIM-1 inside the Ultem matrix at low PIM-1 loadings. Nevertheless, the miscibility of the membranes decreases when the PIM-1 concentration increases.

DSC scans were conducted on these flat sheet membranes to obtain the T_gs of all blends The T_g of PIM-1 is difficult to observe as it is higher than its decomposition temperature[36]; therefore, only the shifts of the Ultem T_g are reported. The T_g shifts from 215°C to 218°C with an increase PIM-1 loading up to 15 wt %, indicating partial miscibility may occur between Ultem and PIM-1 at low PIM-1 loadings. Other characterizations such as AFM and FTIR on flat sheet membranes can be found from our previous study.[26]

Effects of take-up speed and air gap distance on Ultem hollow fibers

As Prof. Koros group has demonstrated the defect-free Ultem hollow fiber,[17,24,25] only limited spinning conditions shown in Table 1 were explored in this study to search for suitable conditions to spin Ultem/PIM-1 hollow fibers. Table 2 tabulates the O_2 and N_2 permeance and O_2/N_2 selectivity of the resultant Ultem hollow fibers as functions of various spinning conditions. The following observation can be summarized.

1. With proper dope formulations and spinning conditions, spinning Ultem/PIM-1 hollow fibers with a defect-free ultrathin dense-selective layer could be easily achievable. Samples UA1, UB1, and UC1 have O_2/N_2 selectivity close to or higher than the intrinsic value of 7.1 with dense-layer thicknesses much lower than 100 nm.

Table 2. The O_2, N_2 Permeance and O_2/N_2 Selectivity of Pristine Ultem Hollow Fibers

Fiber ID	Permeance (GPU) O_2	Permeance (GPU) N_2	Selectivity O_2/N_2	Selective Layer Thickness (nm)
Ultem flat sheet[26]	0.38 Barrer	0.054 Barrer	7.1	–
UA1	5.39	0.77	**7.0**	**71**
UA2	7.07	1.45	5.3	54
UB1	5.22	0.71	**7.4**	**73**
UB2	6.52	1.19	5.5	58
UC1	4.69	0.64	**7.3**	**81**
UC2	7.43	1.46	5.1	51
UD	21.95	14.63	1.5	–

2. Fibers spun from a short air gap distance of 4 cm with a bore-fluid flow rate of 1.5 mL/min were not stable and showed irregular shapes. This was due to rapid solvent exchange, uneven shrinkage, and buckling.[37] To balance the stresses, the bore-fluid flow rate was increased to 3 mL/min during the spinning.

3. No defect-free hollow fibers could be produced when the outer-layer dope flow rate was reduced to 0.4 mL/min (Sample UD).

Tables 1 and 2 also exhibit the effects of take-up speed and air gap distance on O_2/N_2 selectivity of the resultant fibers. With fixed air gaps at 4, 7, and 10 cm, a higher take-up speed could over-stretch polymer chains, result in defects, and reduce selectivity. This phenomenon is consistent with other studies.[38] When take-up speed was maintained at 21.8 m/min, UA2 and UB1 display the effects of air gap distance on O_2/N_2 selectivity. At a high air gap of 10 cm, the resultant membrane shows a high selectivity owing to the proper THF evaporation along the air-gap region[39] as well as chain orientation induced by the spin-line stresses.[38,40] In contrast, fibers spun at an air gap of 7 cm show a reduced selectivity possibly because of uncompleted THF evaporation and less chain orientation induced along the air-gap region.

Figure 5 shows the morphology of Ultem fibers spun at the same take-up speed (UA2, UB1, and UC1). Compared to UA2 and UB1 fibers, UC1 has a thinner fiber wall because it was spun from a larger bore-fluid flow rate. In addition, the latter has a much thinner outer layer than the former. Clearly, a higher bore-fluid flow rate not only can balance the hoop stresses near the spinneret but also accelerate the mass transport and thus assist a faster skin formation.[41,42] In addition, a high bore-fluid flow rate may expand the nascent fiber and form a more oriented outer skin. Therefore, fibers spun from an air gap of 4 cm possess a high selectivity despite of a short air gap distance.

Hollow fiber morphology

Based on the selected spinning conditions (i.e., UA1, UB1, and UC1 as underlined in Table 2) for the pristine Ultem, Ultem/PIM-1 hollow fibers were fabricated at these conditions using three different PIM-1 loadings: 5, 10, and 15 wt % as shown in Table 3. The hollow fibers were, therefore, denoted as 5A, 5B, and 5C for Ultem/PIM-1 (95/5) fibers spun under conditions A, B, and C, respectively. So do 10A, 10B, and 10C for Ultem/PIM-1 (90/10) fibers and 15A, 15B, and 15C for Ultem/PIM-1 (85/15) fibers.

In general, the Ultem/PIM-1 fibers obtained from this study have a round-shape morphology as presented in Figure

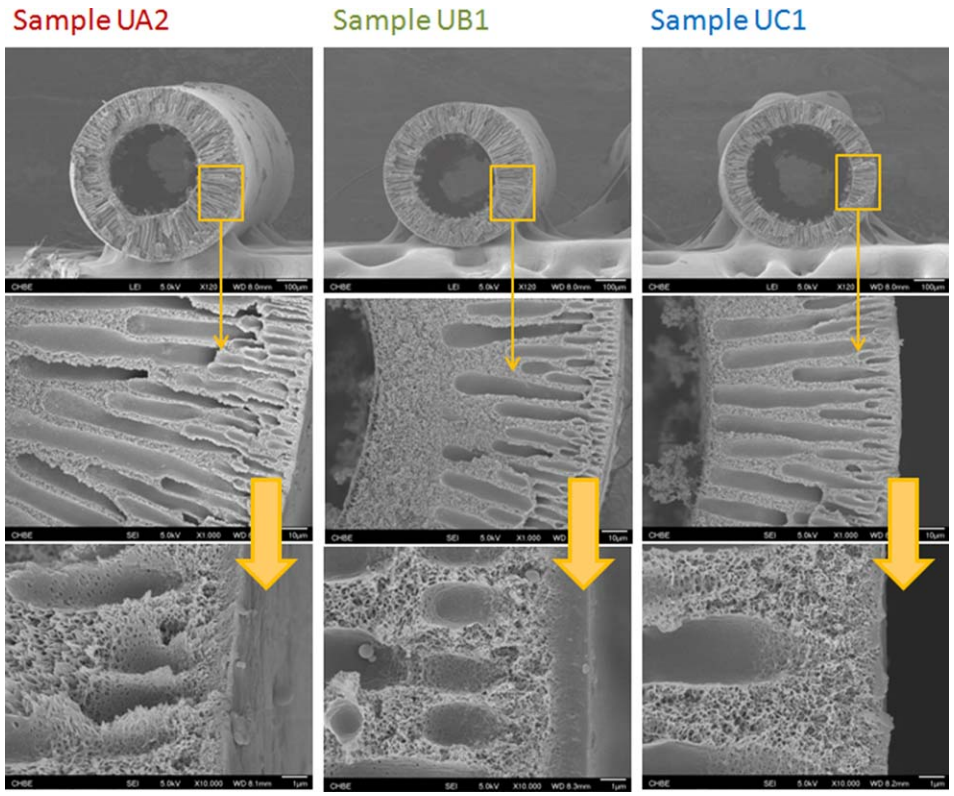

Figure 5. FESEM images for pristine Ultem hollow fibers under spinning conditions UA2, UB1, and UC1 (take-up speed fixed at 21.8 m/min).

[Color figure can be viewed in the online issue, which is available at wileyonlinelibrary.com.]

6. The inner layer of the fibers serves as the mechanical support. It contains finger-like macrovoids to minimize the sublayer resistance for gas transport.

Table 4 shows the detailed gas transport properties of the Ultem/PIM-1 hollow fibers as a function of PIM-1 loading and the calculated selective layer thickness based on the O_2 permeance and permeability. There is a jump in the outer skin thickness from less than 80 nm to over 100 nm when PIM-1 loading increases from 5 to 10 wt %, which might be contributed by two factors. As shown in Figure 2, the dope viscosity is not exactly the same for these Ultem/PIM dopes. As a consequence, the resultant fibers may have experienced different shear rates when extruding from the spinneret and have different degrees of molecular orientation. As the O_2 permeability in Eq. 3 was measured using standard unoriented dense membranes, the calculated apparent dense layer thickness would appear thicker. The other possible reason is due to the reduced miscibility when PIM-1 loading is greater than or equal to 10 wt %. The reduced miscibility may create higher interface resistance between the inner and outer layer, thus slows down the gas permeance. As a result, the calculated apparent dense layer thickness appears to be thicker.

To verify the calculated thickness of the selective layer, PAS analyses were conducted for fibers spun under condition B as illustrated in Figure 7. *S*-parameter is a combined measurement of free volume hole size and its intensity, which can reveal the free volume changes along the cross-section

Table 3. The Spinning Conditions for Different Ultem/PIM-1 Compositions

Outer Dope Composition (wt %)			
Ultem/PIM-1 (95/5)	Ultem/PIM-1/NMP/THF (27.08/1.42/35.8/35.8)		
Ultem/PIM-1 (90/10)	Ultem/PIM-1/NMP/THF (24.75/2.75/36.3/36.3)		
Ultem/PIM-1 (85/15)	Ultem/PIM-1/NMP/THF (21.10/3.72/37.6/37.6)		
Inner dope composition (wt %)	Ultem/NMP (23/77)		
Bore fluid composition (wt %)	NMP/water (95/5)		
External coagulant	Tap water		
Spinneret dimension (mm)	Dual-layer 1.6 no indent		
Spinning temperature (°C)	25 ± 2		
Spinning Condition	**A**	**B**	**C**
Outer dope flow rate (mL/min)	0.6	0.6	0.6
Inner dope flow rate (mL/min)	3.5	3.5	3.5
Bore flow rate (mL/min)	1.5	1.5	3.0
Air gap (cm)	7	10	4
Take-up speed (reading)	16.2	21.8	21.8

Table 4. The Gas Permeance and Selectivity as well as the Apparent Dense Layer Thickness of Ultem/PIM-1 Hollow Fibers

	Permeance (GPU)				Selectivity			
Fiber ID	O_2	N_2	CH_4	CO_2	O_2/N_2	CO_2/N_2	CO_2/CH_4	Selective Layer Thickness (nm)
Ultem dense film[a]	0.38	0.054	0.04	1.48	7.1	27.4	37.0	
UA1	5.39	0.77	0.62	22.8	7.0	29.6	36.6	71
UB1	5.22	0.71	0.65	24.1	7.4	33.9	36.8	73
UC1	4.69	0.64	0.59	21.5	7.3	33.5	36.5	81
Ultem/5%PIM-1 dense film[a]	0.58	0.083	0.06	2.18	7.0	26.2	36.5	
5A	7.36	1.05	0.84	29.4	7.0	28.0	35.2	79
5B	8.19	1.14	0.94	33.9	7.2	29.7	36.1	71
5C	7.82	1.11	0.95	33.6	7.1	30.3	35.3	74
Ultem/10%PIM-1 dense film[a]	1.10	0.16	0.12	3.95	6.8	25.2	33.8	
10A	9.41	1.62	1.27	38.2	5.8	23.6	30.1	117
10B	10.22	1.64	1.27	41.4	6.3	25.2	32.6	108
10C	9.86	1.67	1.29	39.7	5.9	23.8	30.8	112
Ultem/15%PIM-1 dense film[b]	1.34	0.21	0.15	5.27	6.5	25.5	34.2	
15A	10.91	2.23	1.85	47.0	4.9	21.1	25.4	124
15B	13.02	2.24	1.70	49.0	5.8	21.9	28.9	104
15C	11.58	2.18	1.84	48.1	5.3	22.0	26.1	117

[a]Permeability shown in Barrer.26
[b]Measured in this study.

of a composite membrane and is typically used to detect the multilayer structures.[43] In the dual-layer hollow fiber system, the top selective layer is much denser than its supporting layer, thus the free volume change of these two sections can be differentiated by *S*-parameter. The thickness of the dense region can be referred to as the point where *S*-parameter reaches a local maximum value after the early region of a stiff slope.[43,44] The mean implantation depth $Z(E_+)$ of the hollow fiber selective layer can be estimated by the equation below

$$Z(E_+)=\left(\frac{40}{\rho}\right)E_+^{1.6} \tag{4}$$

where Z refers to the mean implantation depth in nm, E_+ stands for the incident energy in keV, and ρ is the density of the material in g/cm^3.[35] According to Figure 7, the mean depth of the fibers is estimated from E_+ equals to 1.5–2.1 keV. The exact incident energy cannot be obtained due to its step increment during data collection. The estimated thickness falls within the range of ~60 nm for fiber UB1 and

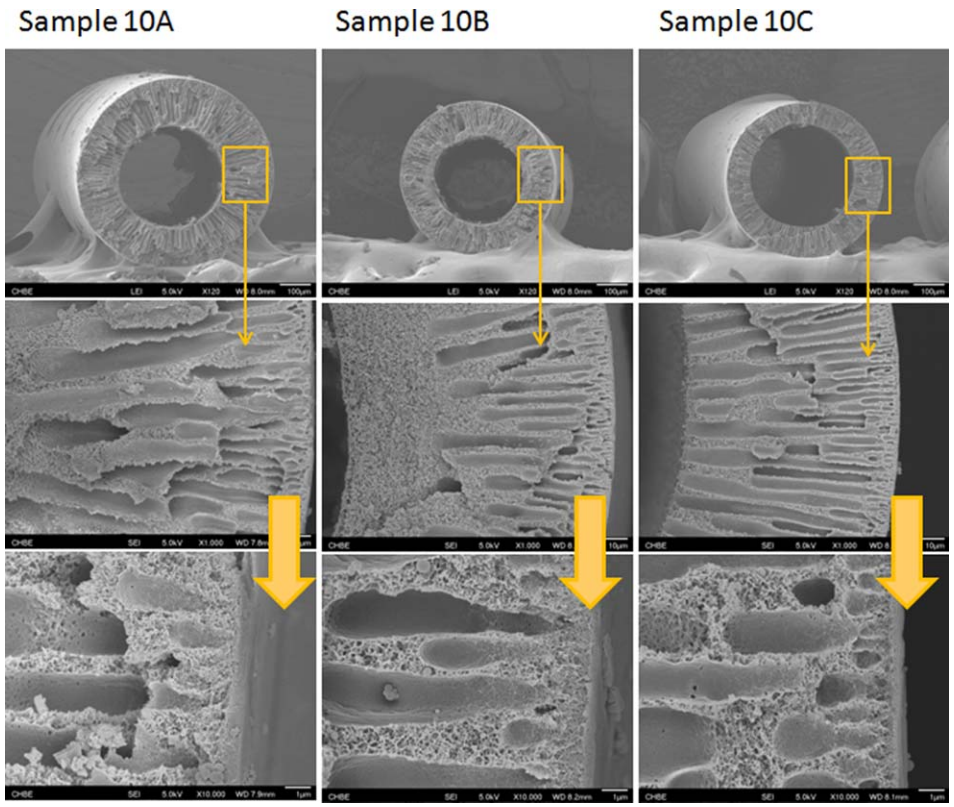

Figure 6. FESEM images for Ultem/PIM-1 (90/10) hollow fibers.

[Color figure can be viewed in the online issue, which is available at wileyonlinelibrary.com.]

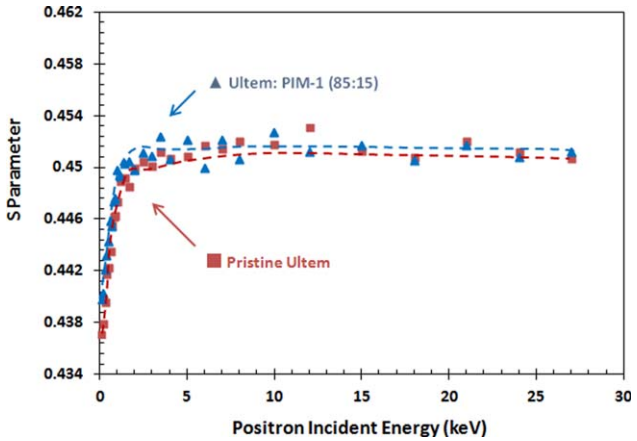

Figure 7. The *S*-parameters of pristine Ultem and Ultem/PIM-1 (85/15) obtained from PAS.

[Color figure can be viewed in the online issue, which is available at wileyonlinelibrary.com.]

~110 nm for fiber 15B, indicating good agreement with the aforementioned calculated thicknesses.

Gas transport properties for Ultem/PIM-1

According to Table 4, the permeance values of all gases increase 50% for all three spinning conditions when only 5 wt % PIM-1 is added into the outer layer. For example, the average permeance of CO_2 increases from 22.8 to 32.3 GPU. Importantly, the selectivity shows no sacrifice and easily surpasses the intrinsic selectivity of flat dense membranes for O_2/N_2 and CO_2/N_2 gas pairs. The CO_2/CH_4 selectivity was slightly below the ideal selectivity but well preserved more than 96% of its intrinsic value.

The gas permeance further increases with increasing PIM-1 loading. With 10 wt % PIM-1 is incorporated inside the outer layer polymer dope, the average O_2 and CO_2 permeance rose to 9.8 and 39.8 GPU, respectively, exhibiting a 75% increment. This is because of a larger fractional free volume is formed in the selective layer with a higher PIM-1 loading. XRD results reported earlier[26] had confirmed this phenomenon where a larger *d*-space value was observed when 10 wt % PIM-1 was added inside the Ultem membranes. As for the selectivity, it is maintained at around 6.3, 25.2, and 32.6 for O_2/N_2, CO_2/N_2, and CO_2/CH_4, respectively, with fibers spun under condition B. These values are very close to those of flat dense membranes (i.e., 6.8, 25.2, and 33.8, respectively), indicating the formation of near defect-free outer layers.

A further increase in PIM-1 loading to 15 wt % produces fibers with an average O_2 permeance of around 12 GPU and CO_2 permeance of nearly 50 GPU. Nevertheless, notable decreases in O_2/N_2, CO_2/N_2, and CO_2/CH_4 selectivity are observed for all fibers. As discussed previously, this may be caused by the reduced miscibility when PIM-1 loading reaches beyond 10 wt %.[26] More chain alignment and orientation may be required to compensate the reduction in their miscibility. Nevertheless, fibers spun under condition B still maintains over 80% of the intrinsic selectivity and displays promising performance.

Figure 8 illustrates the evolution of permeance and selectivity as a function of PIM loading. Compared to other fibers, fibers 5B, 10B, and 15B spun under condition UB1 are nearly defect free probably because of balanced spinning conditions with a higher air gap distance. Therefore, one can conclude that even though Ultem is a low permeable material, its gas permeation can be significantly enhanced by adding a minimum amount of a high free volume material

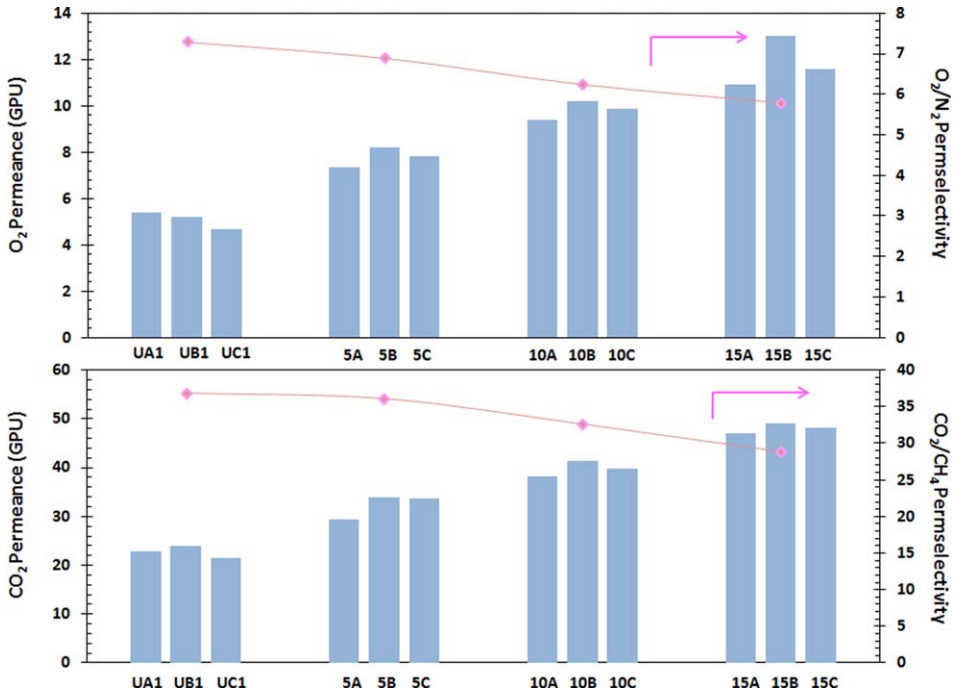

Figure 8. (Upper) the average O_2 permeance of different fibers and the O_2/N_2 selectivity of UB, 5B, 10B, and 15B; (Lower) the average CO_2 permeance of different fibers and the CO_2/CH_4 selectivity of UB, 5B, 10B, and 15B.

[Color figure can be viewed in the online issue, which is available at wileyonlinelibrary.com.]

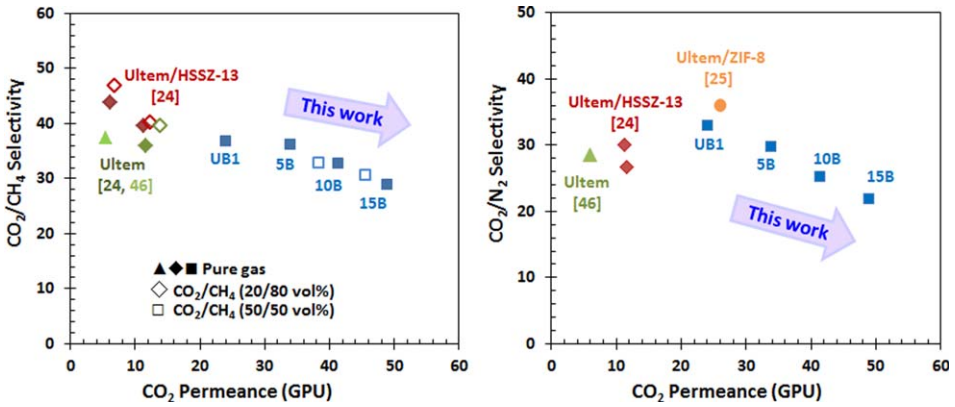

Figure 9. Comparison amongst different Ultem-based hollow fibers for gas separation.

Permeance and selectivity values of Ultem[46] was an estimation. [Color figure can be viewed in the online issue, which is available at wileyonlinelibrary.com.]

without much sacrifice in its gas selectivity if the spinning conditions are properly designed.

Silicone rubber coating was lastly attempted to recover fiber properties spun under conditions 15A and 15C due to their relatively lower selectivity. Although the CO_2/CH_4 selectivity can be recovered to above 31, the CO_2 permeance drops to around 35 GPU for both cases. A recent paper by Huang et al. illustrated the effects of pressure ratio on system performance where a high selectivity does not necessarily improve the energy efficiency in industrial applications.[45] Therefore, gas separation membranes with a high permeance but a reasonable selectivity may have greater industrial potential. Silicone rubber coating may not be necessary for these fibers containing a 15 wt % PIM-1 loading.

Benchmark with other Ultem-based hollow fibers

Figure 9 displays the Ultem-based hollow fibers for CO_2/CH_4 and CO_2/N_2 separation[24,25,46] including the mixed gas data for 10B and 15B using a mixed gas of 50/50 vol % CO_2/CH_4 as the feed. The Ultem fibers generally show good CO_2/CH_4 and CO_2/N_2 selectivity with a relatively low CO_2 permeance. The obtained Ultem fiber permeance in this study is higher than those in the literature. This may be contributed by the optimization of spinning conditions as well as the controlling of dope formulations. With a 15 wt % PIM-1 loading, more than 100% increment in gas permeance is achieved.

In terms of mixed gas data, the CO_2/CH_4 selectivity remains slightly higher than the pure gas data with trivial sacrifice of the permeance. This selectivity increment in mixed gas systems was also observed by other studies,[24,26] which might be contributed from the effect of a higher CO_2 sorption selectivity on the membranes in the competitive sorption process.

Other than the superior separation performance, the newly developed dual-layer fibers ensure a small usage of the expensive material PIM-1. Based on the PIM-1 consumption per unit fiber as expressed in Eq. 5 using the Ultem/PIM-1 (95/5) fiber as an example, the hollow fiber only consists of 0.88 wt % PIM-1 in the overall material while the rest 99.12 wt % is Ultem. With the insubstantial amounts of PIM-1 added, that is, 0.88, 1.7, and 2.3 wt % for Ultem/PIM-1 (95/5), (90/10), and (85/15) fibers, respectively, the fibers demonstrate great improvements on gas permeance

$$\text{PIM-1}_{\text{per unit fiber}} = \frac{\text{PIM-1}_{\text{outer}}}{\text{Polymer}_{\text{outer}} + \text{Polymer}_{\text{inner}}} = \frac{0.6 \times 28.5 \text{ wt\%} \times 5 \text{ wt\%}}{0.6 \times 28.5 \text{ wt\%} + 3.5 \times 23 \text{ wt\%}} \quad (5)$$

Compared to the MMMs consisting of zeolite and MOF, adding HSSZ-13 increases the fiber selectivity with the compensation of its permeance,[17,24] while adding ZIF-8 demonstrates increments in both permeance and selectivity with the aid of the post thermal treatment.[25] In addition, although PIM-1/Matrimid single-layer hollow fibers possess a higher permeance with a similar selectivity,[22] the large amount of PIM-1 used in the fiber reduces its competiveness. On the contrary, the dual-layer hollow fiber developed in this study not only effectively improves the gas transport properties, but also significantly reduces the usage of the expensive material. Thus, this work may open up opportunities for Ultem-based materials in various industrial applications.

Conclusion

Dual-layer Ultem/PIM-1 hollow fibers containing 5–15 wt % PIM-I in the outer selective layer have been fabricated through the dual-layer spinning technology. The following conclusions can be made from the studies of their morphology and gas transport properties:

1. Defect-free dual-layer hollow fibers were successfully fabricated under several spinning conditions. With an addition of 5 wt % PIM-1 in the selective layer, the fibers show a 50% increment in O_2 and CO_2 permeance while maintaining the O_2/N_2 and CO_2/CH_4 selectivity at around 7 and 36, respectively. A further increase in PIM-1 loading toward 15 wt % pushes the CO_2 permeance till 49.0 GPU but the CO_2/CH_4 selectivity slightly drops to around 28.9.

2. The dense layer thicknesses of the newly developed fibers are estimated to be between 70 and 120 nm, indicating the successful formation of ultrathin selective layers. A higher PIM-1 loading tends to increase the dense layer thickness. These thickness values are further verified by PAS measurements with good agreements.

3. Mixed gas results of Ultem/PIM-1 hollow fibers 10B and 15B exhibit slightly higher CO_2/CH_4 selectivity without much compromising gas permeance due to the better CO_2 affinity contributed by PIM-1.

4. The dual-layer coextrusion technology ensures an extremely low usage of the expensive material in the

resultant fibers. Only 0.88, 1.7, and 2.3 wt % PIM-1 of the total polymeric materials were consumed in the fibers of Ultem/PIM-1 (95/5), Ultem/PIM-1 (90/10), and Ultem/PIM-1 (85/15), respectively.

5. In summary, 5B, 10B, and 15B spun under condition UB1 are nearly defect free as a result of balanced spinning conditions with a higher air gap distance. Under properly designed spinning conditions, the permeance of Ultem, a low permeable material, can be considerably improved by incorporating a minimum amount of a high free volume material without much sacrifice in its gas selectivity.

Acknowledgments

This project is supported by the National Research Foundation, Prime Minister's Office, Singapore under its Competitive Research Program (CRP Award number NRF-CRP 5-2009-5 (NUS grant number R-279-000-311-281)). The authors would like to thank Dr. Hangzheng Chen, Mr. Yupan Tang, and Ms. Wai Fen Yong for their kind help and valuable suggestions.

Literature Cited

1. He X, Hägg MB. Hollow fiber carbon membranes: investigations for CO2 capture. *J Membr Sci*. 2011;378:1–9.
2. Baker RW, Lokhandwala K. Natural gas processing with membranes: an overview. *Ind Eng Chem Res*. 2008;47:2109–2121.
3. Wang H, Werth S, Schiestel T, Caro J. Perovskite hollow-fiber membranes for the production of oxygen-enriched air. *Angew Chem Int Ed*. 2005;44:6906–6909.
4. Peng N, Widjojo N, Sukitpaneenit P, Teoh MM, Lipscomb GG, Chung TS, Lai JY. Evolution of polymeric hollow fibers as sustainable technologies: past, present, and future. *Prog Polym Sci*. 2012; 37:1401–1424.
5. Pinnau I, Koros WJ. Defect-free ultrahigh flux asymmetric membranes, US Patent 4,902,422, 1990.
6. Li DF, Chung TS, Wang R. Morphological aspects and structure control of dual-layer asymmetric hollow fiber membranes formed by a simultaneous co-extrusion approach. *J Membr Sci*. 2004;243:155–175.
7. Lipscomb GG. The melt hollow fiber spinning process: steady-state behavior, sensitivity and stability. *Polym Adv Technol*. 1994;5:745–758.
8. Shang M, Matsuyama H, Teramoto M, Lloyd DR, Kubota N. Preparation and membrane performance of poly(ethylene-co-vinyl alcohol) hollow fiber membrane via thermally induced phase separation. *Polymer*. 2003;44:7441–7447.
9. Kesting RE, Fritzsche AK, Murphy MK, Cruse CA, Handermann AC, Malon RF, Moore MD. The second-generation polysulfone gas-separation membrane. I. The use of lewis acid: base complexes as transient templates to increase free volume. *J Appl Polym Sci*. 1990; 40:1557–1574.
10. Chung TS, Kafchinski ER, Vora R. Development of a defect-free 6FDA-durene asymmetric hollow fiber and its composite hollow fibers. *J Membr Sci*. 1994;88:21–36.
11. Clausi DT, Koros WJ. Formation of defect-free polyimide hollow fiber membranes for gas separations. *J Membr Sci*. 2000;167:79–89.
12. Chung TS. Fabrication of hollow-fiber membranes by phase inversion. In: Li NN, Fane AG, Ho WSW, Matsuura T, editors. *Advanced Membrane Technology and Applications, Chapter 31*. Hoboken, NJ: Wiley, 2008.
13. Peng N, Chung TS, Chng ML, Aw W. Evolution of ultra-thin dense-selective layer from single-layer to dual-layer hollow fibers using novel Extem® polyetherimide for gas separation. *J Membr Sci*. 2010;360:48–57.
14. Yanagimoto T. Method for manufacture of hollow-fiber porous membranes, Japanese Patent 63,092,712, 1988.
15. Ekiner OM, Hayes RA, Manos P. Novel multicomponent fluid separation membranes, US Patent 5,085,676, 1992.
16. Li DF, Chung TS, Wang R, Liu Y. Fabrication of fluoropolyimide/polyethersulfone (PES) dual-layer asymmetric hollow fiber membranes for gas separation. *J Membr Sci*. 2002;198:211–223.
17. Husain S. Mixed matrix dual layer hollow fiber membranes for natural gas separation, Ph.D. Dissertation, Georgia Institute of Technology, Atlanta, GA, 2006.
18. Kneifel K, Peinemann KV. Preparation of hollow fiber membranes from polyetherimide for gas separation. *J Membr Sci*. 1992;65:295–307.
19. Wang Y, Jiang LY, Matsuura T, Chung TS, Goh SH. Investigation of the fundamental differences between polyamide-imide (PAI) and polyetherimide (PEI) membranes for isopropanol dehydration via pervaporation. *J Membr Sci*. 2008;318:217–226.
20. Visser T, Wessling M. Auto and mutual plasticization in single and mixed gas C_3 transport through Matrimid-based hollow fiber membranes. *J Membr Sci*. 2008;312:84–96.
21. Jiang LY, Song ZW. Interfacial resistance of dual-layer asymmetric hollow fiber pervaporation membranes formed by co-extrusion. *J Polym Res*. 2011;18:2505–2514.
22. Yong WF, Li FY, Xiao YC, Chung TS, Tong YW. High performance PIM-1/Matrimid hollow fiber membranes for CO_2/CH_4, O_2/N_2 and CO_2/N_2 separation, *J Membr Sci*. 2013;443:156–169.
23. Jiang LY, Chung TS, Rajagopalan R. Matrimid®/MgO mixed matrix membranes for pervaporation. *AIChE J*. 2007;53:1745–1757.
24. Husain S, Koros WJ. Mixed matrix hollow fiber membranes made with modified HSSZ-13 zeolite in polyetherimide polymer matrix for gas separation. *J Membr Sci*. 2007;288:195–207.
25. Dai Y, Johnson JR, Karvan O, Sholl DS, Koros WJ. Ultem®/ZIF-8 mixed matrix hollow fiber membranes for CO_2/N_2 separation. *J Membr Sci*. 2012;401–402:76–82.
26. Hao L, Li P, Chung TS. PIM-1 as an organic filler to enhance the gas separation performance of Ultem polyetherimide. *J Membr Sci*. 2014;453:614–623.
27. McKeown NB, Budd PM, Msayib K, Ghanem B. Microporous polymer material, International Patent WO05012397,2005.
28. Budd PM, Elabas ES, Ghanem BS, Makhseed S, McKeown NB, Msayib KJ, Tattershall CE, Wong D. Solution-processed, organophilic membrane derived from a polymer of intrinsic microporosity. *Adv Mater*. 2004;16:456–459.
29. Zuo J, Wang Y, Chung TS. Novel organic-inorganic thin film composite membranes with separation performance surpassing ceramic membranes for isopropanol dehydration. *J Membr Sci*. 2013;433:60–71.
30. Chung TS, Teoh SK, Hu X. Formation and ultrathin high-performance polyethersulfone hollow-fiber membranes. *J Membr Sci*. 1997;133:161–175.
31. Ren JZ, Chung TS, Li DF, Wang R, Liu Y. Development of asymmetric 6FDA- 2, 6 DAT hollow fiber membranes for CO_2/CH_4 separation: 1. The influence of dope composition and rheology on membrane morphology and separation performance. *J Membr Sci*. 2002;207:227–240.
32. Chung TS, Teoh SK. Breaking the limitation of composition change during isothermal mass-transfer processes at the spinodal. *J Membr Sci*. 1997;130:141–147.
33. Li FY, Li Y, Chung TS, Chen H, Jean YC, Kawi S. Development and positron annihilation spectroscopy (PAS) characterization of polyamide imide (PAI)–polyethersulfone (PES) based defect-free dual-layer hollow fiber membranes with an ultrathin dense-selective layer for gas separation. *J Membr Sci*. 2011;378:541–550.
34. Cao C, Chung TS, Chen SB, Dong ZJ. The study of elongation and shear rates in spinning process and its effect on gas separation performance of Poly(ether sulfone) (PES) hollow fiber membranes. *Chem Eng Sci*. 2004;59:1053–1062.
35. Jean YC, Mallon PE, Schrader DM. *Principle and Application of Positron & Positronium Chemistry*. Singapore: World Scientific, 2002.
36. Du N, Park HB, Robertson GP, Dal-Cin MM, Visser T, Scoles L, Guiver MD. Polymer nanosieve membranes for CO2-capture applications. *Nat Mater*. 2011;10:372–375.
37. Bonyadi S, Chung TS, Krantz WB. Investigation of corrugation phenomenon in the inner contour of hollow fibers during the non-solvent induced phase-separation process. *J Membr Sci*. 2007;299: 200–210.
38. Peng N, Chung TS. The effects of spinneret dimension and hollow fiber dimension on gas separation performance of ultra-thin defect-free Torlon® hollow fiber membranes. *J Membr Sci*. 2008;310:455–465.
39. Shilton SJ. Forced convection spinning of hollow fibre membranes: modelling of mass transfer in the dry gap, and prediction of active

layer thickness and depth of orientation. *Sep Purif Technol*. 2013; 118:620–626.
40. Chung TS. The limitations of using Flory-Huggins equation for the states of solutions during asymmetric hollow fiber formation. *J Membr Sci*. 1997;126:19–34.
41. Pereira CC, Nobrega R, Peinemann KV, Borges CP. Hollow fiber membranes obtained by simultaneous spinning of two polymer solutions: a morphological study. *J Membr Sci*. 2003;226:35–50.
42. Gordeyev SA, Shilton SJ. Forced convection spinning of gas separation hollow fiber membranes: some underlying factors, mechanisms and effects. *J Membr Sci*. 2004;229:225–233.
43. Kao ST, Huang SH, Liaw DJ, Chao WC, Hu CC, Li CL, Wang DM, Lee KR, Lai JY. Interfacially Polymerized thin-film composite polyamide membrane: positron annihilation spectroscopic study, characterization and pervaporation performance. *Polym J*. 2010;42:242–248.
44. Zuo J, Wang Y, Sun SP, Chung TS. Molecular design of thin film composite (TFC) hollow fiber membranes for isopropanol dehydration via pervaporation. *J Membr Sci*. 2012;405–406:123–133.
45. Huang Y, Merkel TC, Baker RW. Pressure ratio and its impact on membrane gas separation processes. *J Membr Sci*. 2014;463:33–40.
46. Wang D, Li K, Teo WK. Preparation and characterization of polyetherimide asymmetric hollow fiber membranes for gas separation. *J Membr Sci*. 1998;138:193–201.

Manuscript received May 16, 2014, and revision received July 10, 2014.